Anterior expansion and posterior addition to the notochord mechanically coordinate embryo axis elongation

S.B.P. McLaren[1] and B. Steventon[1]

[1] Department of Genetics, University of Cambridge, United Kingdom

Abstract

During development the embryonic body axis progressively elongates from head-to-tail along the anterior-posterior (AP) axis. It is known that multiple tissues contribute to embryo elongation, but how force generated by tissue morphogenesis leads to axis elongation is not well understood. The notochord, a rod-shaped tissue possessed by all vertebrates, runs across the entire length of the somitic compartment and is flanked on either side by the developing somites in the segmented region of the axis and presomitic mesoderm in the posterior region. Cells in the notochord undergo an expansion that is constrained by a stiff sheath of extracellular matrix, thought to increase the internal pressure in the notochord allowing it to straighten and elongate the embryo. Therefore, it is appropriately positioned to play a role in mechanically elongating the somitic compartment. Here, we use multi-photon mediated cell ablation to remove specific regions of the developing notochord and quantify the impact on axial elongation. We show that notochord cell expansion generates a force that displaces notochord cells relative to adjacent axial tissues and contributes to the elongation of segmented tissue during post-tailbud stages of development. Crucially, the posterior notochord provides resistance to anterior notochord cell expansion and thereby allows for force generation across the AP axis. Therefore, notochord formation and maturation act as temporally coordinated morphogenetic events that together shape the zebrafish embryo AP axis.

Introduction

The formation of complex body shapes is a central question in developmental biology. A key component of body shape formation is the elongation of the embryo head-to-tail, or anterior-posterior (AP) axis. Whilst the biochemical players in this process have been studied in detail, axis elongation is largely a physical process requiring multiple axial tissues to change shape as they undergo morphogenesis in order to achieve an elongated AP axis (Bénazéraf et al., 2017; Steventon et al., 2016, Xiong et al., 2020). Disrupting the morphogenesis of one of these tissues, the notochord, results in a truncated axis, which can lead to severe defects such as skeletal malformations (Bagwell et al., 2020; Ellis et al., 2013). Running through the middle of the embryo and spanning the length of the segmented and unsegmented regions of the AP axis, the notochord is a defining structure of the developing vertebrate embryo (Stemple, 2005). Studies in Xenopus embryos have identified the constrained expansion of cells within the notochord to lead to an increase in notochord stiffness as the embryo develops, making it a candidate tissue for driving the physical deformation of surrounding tissues that may be required for axis elongation (Adams et al., 1990). In addition, measurements of volumetric tissue growth in the developing zebrafish embryo have revealed a progressive increase in notochord volume, that, combined with the excellent live imaging capacity and fast development of the zebrafish embryo make this an appropriate system for investigating the physical impact of notochord morphogenesis on surrounding axial tissues (Steventon et al., 2016).

The notochord is flanked on either side by blocks of tissue called somites, the first of which are established prior to notochord volume increase (Steventon et al., 2016). Further somites are formed as unsegmented tissue (the presomitic mesoderm) in the posteriorly located tailbud gets progressively segmented (Gomez et al., 2008; Oates et al., 2012). Concomitant with tailbud derived somite formation, notochord volume begins to increase as inner notochord cells develop vacuoles which expand over time(Steventon et al., 2016) (Ellis et al., 2013). Newly formed somites undergo changes in shape as they mature, and take up a characteristic ‘chevron’ shape, with typically 30 to 34 somites being formed in total (Kimmel et al., 1995; Rost et al., 2014), and the physical coupling between somites and the notochord is thought to change as somites mature (Tlili et al., 2019). Whilst elongation driven by the segmentation of tailbud derived tissue into somites has been studied (Das et al., 2019; Dray et al., 2013; Lawton et al., 2013; Mongera et al., 2018; Steventon et al., 2016), the contribution of mature somite elongation to axis elongation is less well understood.

At the posterior tip of the notochord a separate morphogenetic event is occurring in which cells are contributed to the differentiated notochord from a population of notochord progenitors, with progenitors stacking up in a characteristic arrangement

to contribute to the notochord rod (Kanki and Ho, 1997). Genetic manipulations that switch the fate of notochord progenitors from notochord to other tissue types are associated with tail elongation defects (Row et al., 2016), establishing that they play a role in this developmental process. But whilst the role of other tailbud-located progenitor populations in elongating the AP axis has been investigated (Goto et al., 2017; Mongera et al., 2018; Attardi et al., 2018), how the posterior contribution of cells from notochord progenitors is coordinated with the expansion of more anterior notochord cells and the combined impact of these processes on axis elongation remains to be determined.

Here, we used a quantitative analysis of embryo AP axis elongation and notochord morphogenesis to investigate which aspects of notochord morphogenesis contribute to AP axis elongation. We show that notochord cell expansion progresses both temporally and spatially as the AP axis straightens and elongates, at the same time as a population of progenitors contributes to the posterior notochord and gets depleted. Using targeted photo-ablations of anterior notochord cells we found that notochord expansion is not a major player in driving segmentation-derived axis elongation during tailbud stages, and that this mode of elongation is extremely robust to perturbation. However, we found that notochord cell expansion contributes to the elongation of segmented tissue that extends the AP axis during post-segmentation stages. This coincides with the emergence of a posteriorly directed movement of expanded notochord cells, which we find is resisted by unexpanded cells in the posterior notochord. A pool of progenitors responsible for the addition of cells to the posterior end of the differentiated notochord gets depleted over time and may act with cell expansion to coordinate elongation along different regions of the axis. Overall, we identify the concomitant expansion of notochord cells beginning in the anterior and progressing posteriorly, and contribution of progenitors to the posterior end of the notochord, as two temporally coordinated morphogenetic events that shape the zebrafish embryo AP axis.

Results and Discussion

Modes of axis elongation change as embryos progress from tailbud stages into post-tailbud stages of development

The onset of a dramatic change in embryo shape coincides with notochord volume increase (Steventon et al., 2016). To quantitatively characterise embryo AP axis elongation occurring concomitantly with notochord volume increase, we imaged developing zebrafish embryos from the onset of notochord vacuolation onwards and quantified elongation in segmented and unsegmented regions of the axis (movie 1). The somitic compartment spans both the trunk and tail regions of the AP axis, with somite boundaries providing clear reference points for demarcating regions of the axis (Fig.1A), previous work has shown that these regions elongate by different

extents (Steventon et al., 2016). Throughout this study we use the somitic compartment as a reference for investigating axis elongation and utilize somite boundaries to demarcate different regions of the axis. Segmented tissue elongation is tracked using the boundaries of 5 formed somites. Length generated from unsegmented tissue is tracked using the posterior-most somite boundary (and later the corresponding more mature somite boundary) and tail-end, thus incorporating newly formed somites as development progresses.

In zebrafish, cells derived from the tailbud contribute to embryo axis elongation through a process of lengthening and thinning (Steventon et al., 2016). The tailbud remains present until the 30-somite stage, when it begins to degenerate (Kimmel et al., 1995). Whilst the contribution of tailbud derived tissue to axis elongation has been studied (Lawton et al., 2013; Mongera et al., 2018; Steventon et al., 2016), less is known about axis elongation after tailbud stages. We therefore compared elongation over a 5-hour period during tailbud (24ss) and post-tailbud and stages (30ss) to investigate the modes of axis elongation utilised during each of these phases of embryo morphogenesis. We found segmented tissue elongation to be minimal during tailbud stages (Fig.1B and D magenta region), with a mean length of approximately 6µm (2.5% increase) being generated from segmented region elongation (Fig.1D). However, in post-tailbud stage embryos mean length increased by approximately 34µm (13% increase) (Fig.1C and E). In contrast to the already segmented region of the body axis, the mean length generated from unsegmented tissue (Fig.1B green region) was approximately 120µm (45% increase) in tailbud stage embryos, and 70µm (36% increase) in post-tailbud stage embryos (Fig.1E). When measuring the length of the whole somitic compartment we found the increase in mean length to be lower than expected based on previous studies (Fig.S1A and B). This is likely to be due to a difference in the way axis length is measured, with our measurements accounting for the unwrapping of the embryo from the yolk that occurs over tailbud stages (Fig S1A and C). To investigate embryo straightening we measured the average curvature of the somitic compartment as well as the trunk and tail regions of the axis. These measurements showed that embryos underwent a dramatic straightening, with the trunk and tail regions of the axis both decreasing in curvature (Figs.1SD and E). Overall, our findings show that embryo AP axis elongation can be described by two phases: straightening of the embryo, accompanied by elongation generated from the segmentation of unsegmented posterior tissue during tailbud stages, followed by elongation of segmented tissue during post-tailbud stages (movie 1).

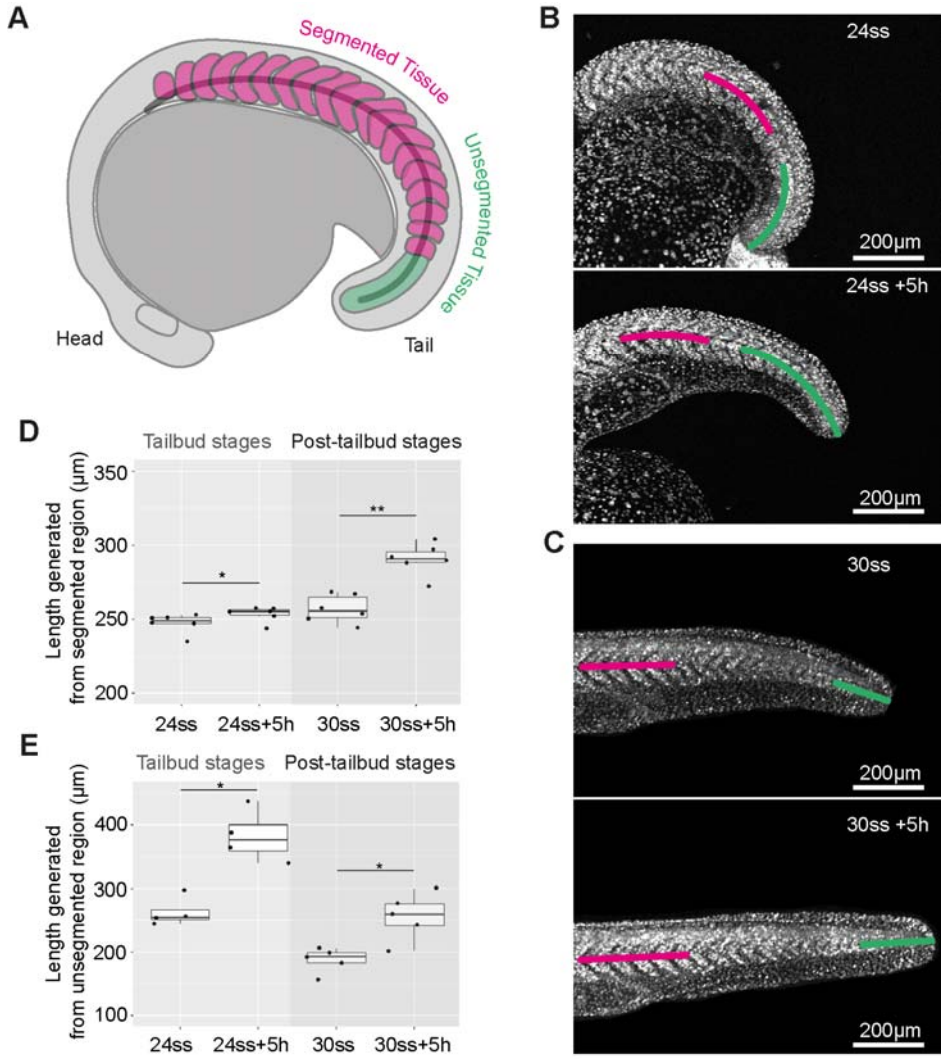

Fig. 1. Axis elongation occurs predominantly in the unsegmented region during tailbud stages and later continues in segmented tissue.

(A) A schematic outlining the segmented and unsegmented regions of the somitic compartment.
(B) Live images of a zebrafish embryo expressing NLS-KikGR at approximately the 24-somite stage and 5 hours later. Length arising from segmented (magenta) and unsegmented (green) tissue during tailbud stages.
(C) Live images of a zebrafish embryo expressing NLS-KikGR at approximately the 30-somite stage and 5 hours later. Length arising from segmented (magenta) and unsegmented (green) tissue during post-tailbud stages.
(D) The length of a region of segmented tissue in tailbud (24ss) and post-tailbud (30ss) embryos and the length generated from this region over 5-hours (n=6 and n=6 respectively, $p<0.05$, $p<0.01$ respectively).
(E) The length of a region of unsegmented tissue in tailbud (24ss) and post-tailbud (30ss) embryos and the length generated from this region over 5-hours (n=4 and n=5 respectively, $p<0.05$, $p<0.05$ respectively).
Curves for calculating segmented (magenta) and unsegmented tissue (green) length are overlaid.
Anterior is to the left and posterior to the right in all images.

Notochord cell expansion leads to the posterior displacement of notochord cells relative to adjacent axial tissues

To gain insight into how notochord morphogenesis may be impacting axis elongation during tailbud and post-tailbud stages of development, we characterised notochord cell expansion by measuring the AP length of vacuoles in live-imaged lifeact-GFP expressing embryos. Measurements of vacuole length were compared both temporally, in an equivalent region of the notochord of different stage embryos (Fig.2A), and spatially, in notochord regions in the anterior vs. the posterior in embryos of the same stage (Fig.2C). In agreement with previous work, we found that notochord cells expanded as development progressed (Bagwell et al., 2020) (Fig.2B), and that vacuoles in more anterior regions had significantly longer AP lengths than those in more posterior regions (Fig.2D). In embryos entering post-tailbud stages, we observed that notochord cells began to move posteriorly relative to neighbouring axial tissues, in contrast to the bi-directional displacement of notochord cells recently observed in Medaka (Seleit et al., 2020) (Fig. 2E and F, movie 2). Manual tracking of more expanded notochord cells in the anterior and less expanded cells in the posterior revealed that the posterior displacement of notochord cells relative to adjacent tissues was greater in regions where notochord cells were more expanded (Figs S2A and B). These findings suggest that notochord cell expansion generates a force that leads to the posterior displacement of notochord cells relative to adjacent axial tissues.

In order to investigate how forces generated from anterior notochord cell expansion might propagate along the AP axis and to neighbouring tissues, a technique is required that allows for precise spatio-temporal removal of notochord cells. To this end, we used multi-photon ablation to cut through cells at defined regions of the AP axis (movie 3), resulting in the destruction of tissue local to the ablation site (Figs.2G and H). Ablation of a region of anterior expanding notochord cells reversed the direction of expanded notochord cell displacement (movie 4), whilst the movement of less expanded posterior notochord cells was less affected (Figs.2I and J). Thus, notochord cell expansion begins at a developmental stage corresponding to the onset of overall embryo straightening and progresses posteriorly along the notochord in a correlated fashion with straightening and tail elongation. As embryos enter post-tailbud stages the continued expansion of cells in the notochord generates a force, displacing neighbouring notochord cells relative to adjacent somites.

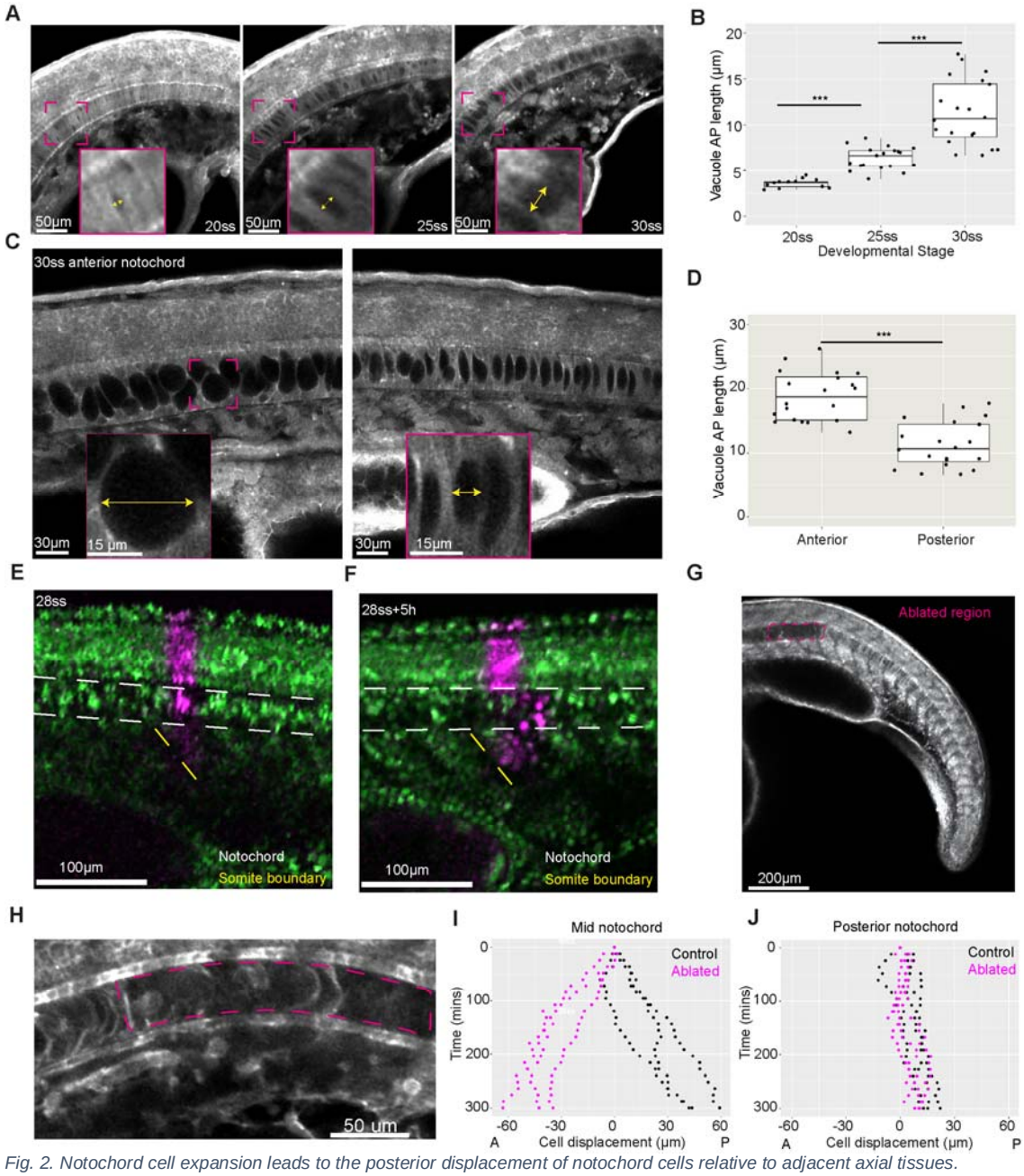

Fig. 2. Notochord cell expansion leads to the posterior displacement of notochord cells relative to adjacent axial tissues.

(A) Images of notochord cells in an equivalent region of an embryo at 20, 25, and 30 somite stages. Yellow arrows indicate direction in which length measurement was taken. Lifeact-GFP reporter signal shown.
(B) AP length of vacuoles in µm in embryos at 20, 25, and 30 somite stages (n=3, n=4 and n=4 embryos respectively, between 3 and 5 vacuoles measured per embryo. $p<0.001$ and $p<0.001$ respectively).
(C) Images of notochord cells in the trunk and tail region of an embryo. Yellow arrows indicate direction in which length measurement was taken. Lifeact-GFP reporter signal shown.
(D) AP length of vacuoles in µm in trunk and tail regions of 30 somite stage embryos (n= 4 embryos, 5 vacuoles measured in the trunk and tail of each embryo. $p<0.001$).
(E) A midline view of a 28-somite stage embryo expressing NLS-KikGR showing a photolabel made in the neural tube, notochord, and somites at the same region of the axis.
(F) A midline view of a 28-somite stage embryo expressing NLS-KikGR showing the photolabel in (E) 5 hours later.
(G) A midline view of an embryo with an anterior notochord ablation.
(H) An image of region of ablated notochord imaged approximately 3 hours after the ablation was performed.
(I) Cell displacement in µm of manually tracked notochord cells in the mid region of the axis of control and notochord ablated embryos (n=3 embryos per condition, 1 cell track per embryo).
(J) Cell displacement in µm of manually tracked notochord cells in the posterior region of the axis of control and notochord ablated embryos (n=3 embryos per condition, 1 cell track per embryo).
Anterior is to the left and posterior to the right in all images.

Notochord cell expansion is a driver of segmented tissue elongation during post-tailbud stages of development

To investigate whether notochord cell expansion impacts on elongation arising from the segmentation of unsegmented tissue in the posterior of the body axis, we performed site-specific ablations of anterior notochord cells just as they were beginning to expand and measured posterior tail elongation during tailbud stages of development (Fig.3A and S3A). We found that posterior tail elongation was not significantly affected in ablated embryos (Fig.3B and C). Strikingly, segmentation-derived elongation could continue in an embryo with almost complete notochord ablation (movie 5), and photolabeling of presomitic mesoderm progenitors revealed that they continued to exit the tailbud in notochord ablated embryos (Fig.3D). To investigate the impact of notochord cell expansion on the straightening of the axis characterised above, we measured the curvature of a 15-somite sample of the axis in control and ablated embryos over time (Fig.S3B). We found that embryo straightening was perturbed in regions where the notochord was ablated (Fig.S3C) suggesting that notochord continuity is required for complete straightening of the axis. Together, these results demonstrate that elongation derived from the segmentation of posterior unsegmented tissue is a robust process that can continue in the absence of notochord cell expansion.

To investigate whether notochord cell expansion impacts post-tailbud stages of axis elongation, we measured the elongation of segmented tissue in embryos with and without anterior notochord ablations from the 30-somite stage (Fig. 3E). The region used for quantifying segmented tissue elongation was located in an equivalent region along the axis in controls and ablated embryos and was positioned posteriorly away from the site of notochord ablation in the ablated case. As characterised above, this region was adjacent to either posteriorly directed notochord cell movement (in controls) or anteriorly directed notochord cell movement (in ablated embryos). The elongation of this region over a period of 5 hours was found to be approximately halved in ablated embryos (Figs.3F and G, movies 6 and 7). Inhibiting notochord cell expansion by blocking vacuolation with Bafilomycin, an inhibitor of vacuolar type H^+-ATPases required for vacuole expansion (Ellis et al., 2013), was also found to reduce elongation in this region of segmented tissue (Fig.S3D). Together these results reveal a role for notochord cell expansion in elongating segmented tissue in post-tailbud stage embryos.

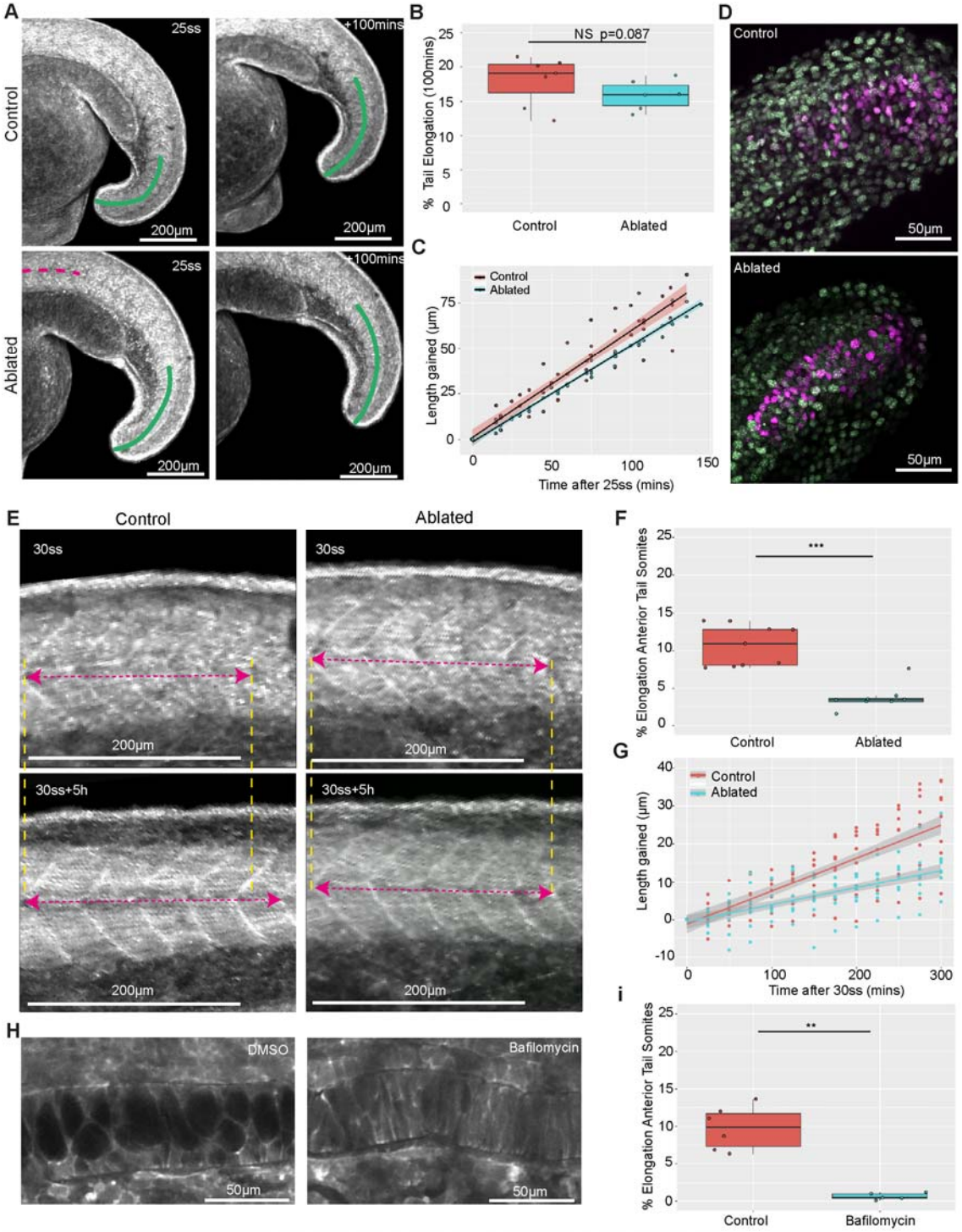

Fig. 3. Notochord cell expansion is a driver of elongation in segmented tissue during post-tailbud stages.

(A) Control and anterior notochord ablated Lifeact-GFP expressing embryos imaged at the 25-somite stage and 100 minutes later. Overlaid curves show the region tracked for elongation measurements. The magenta dashed line indicates the region where the notochord is ablated.
(B) Percentage elongation of the tail region in control and ablated embryos over 100 minutes (n=7 control embryos, n=6 ablated embryos, p=0.087).
(C) Length gained in the tail region of control and ablated embryos over time in tailbud stage embryos.
(D) Photolabels of presomitic mesoderm progenitors in control and ablated embryos imaged 4 hours after the time of labelling. (n=4 control and n=5 ablated embryos).
(E) Elongation of a region of 5 anterior tail somites in control and ablated post-tailbud stage embryos (visualised in a Lifeact-GFP reporter line).

(F) Percentage elongation of a region of 5 anterior tail somites in control and ablated post-tailbud stage embryos over a period of 5 hours (n=9 control and n=8 ablated embryos, $p<0.001$)
(G) Length gained in a region of 5 somites in control and ablated post-tailbud stage embryos over time.
(H) Images of a dmso treated control notochord and Bafilomycin treated embryo notochord visualised in a lifeact-GFP reporter line.
(I) Percentage elongation of a region of 5 anterior tail somites in control and Bafilomycin treated embryos over a period of 3 hours (n=6 control and n=5 Bafilomycin treated embryos, $p<0.01$).
Anterior is to the left and posterior to the right in all images.

Notochord progenitors provide a source of resistance to anterior notochord cell expansion that facilitates the elongation of segmented tissue

The expansion of notochord cells has previously been shown to be constrained by a stiff notochord sheath that circumferentially wraps the notochord (Adams et al., 1990). However, it is not well understood whether and how notochord cell expansion is constrained in the AP direction. We observed a posterior displacement of notochord cells in regions where they become expanded, however, less expanded notochord cells in the posterior did not move as much relative to surrounding tissues. These less expanded posterior notochord cells are derived from a population of notochord progenitors, located in the posterior of the embryo. We wondered if the addition of unexpanded cells to the posterior notochord was coordinated with the progression of notochord cell expansion posteriorly along the axis. To investigate this, we used the expression of *flh* to mark the notochord progenitor domain and measured the volume of the domain at different stages of development (Fig. 4A). This revealed a decrease in notochord progenitor domain volume as development progressed (Fig. 4C). To investigate whether this volume decrease corresponded to a change in the contribution of cells to the posterior end of the notochord we photolabelled the notochord progenitor domain in embryos during tailbud stages (16ss) and post-tailbud stages (30ss) and tracked the length of the label over time (Fig. 4B). The percentage increase in label length was found to be lower in post-tailbud stage embryos compared to embryos in tailbud stages (Fig.4D). Together these results show that the notochord progenitor pool is depleted over time and that less length is contributed to the posterior notochord in later stages of development. Previous work has shown that early termination of progenitor addition to the notochord is associated with AP axis elongation defects (Row et al., 2016). We attempted to prevent the contribution of new cells to the posterior notochord by ablating the notochord progenitor population (Fig. S4A). Intriguingly, we found that, whilst axis elongation defects occurred (Fig. S4B), the notochord progenitor pool was able to regenerate after ablation and recover the posterior notochord (Figs. S4D and E). By tracking elongation in the region where the posterior notochord had been recovered, we found that elongation resulting from the segmentation of the final few somites was unaffected in this recovered region (Figs. S4C and F). These findings highlight the robustness of posterior processes that contribute to axis elongation, both in terms of cell contribution to the posterior notochord and segmentation derived elongation.

Given that the notochord was regenerated after notochord progenitor ablation, we decided to focus our perturbations on the already formed posterior notochord. In embryos entering post-tailbud stages of development notochord cell expansion has progressed posteriorly along the axis to approximately the anterior tail region (close to the end of the yolk extension), where it meets the unexpanded notochord cells. To investigate whether unexpanded notochord cells are subject to a posteriorly directed pushing force generated by anterior notochord cell expansion, we imaged the nuclei of unexpanded notochord cells in this region in control embryos, and just posterior to an ablation site in ablated embryos (Fig. 4E). We found that nuclei in control embryos were angled towards the posterior, whereas nuclei posterior to an ablation site were angled towards the anterior (Fig.4F and G). These findings suggest that unexpanded notochord cells are being deformed by a posteriorly directed force arising from notochord cell expansion.

To investigate whether unexpanded posterior notochord cells provided a source of resistance to notochord cell expansion, we ablated posterior unexpanded notochord cells in embryos at post-tailbud stages (Fig. 4H). Manual tracking of expanding notochord cells just anterior to the ablation site, revealed that the posterior displacement of these cells was increased in ablated embryos compared to controls (Fig. 4I and K) (movies 8 and 9). Finally, to check whether resistance provided by posterior unexpanded notochord cells contributed to the elongation of segmented tissue, we measured the elongation of a region of somites anterior to the site of ablation (in an equivalent to that used in previous ablation experiments) (Fig. 4J). We found that the elongation of this region was also decreased in ablated embryos (Fig. 4L). These results suggest that posterior notochord cells provide a source of resistance to notochord cell expansion and that this may generate a stretch along the AP axis, deforming segmented tissue in post-tailbud stage embryos.

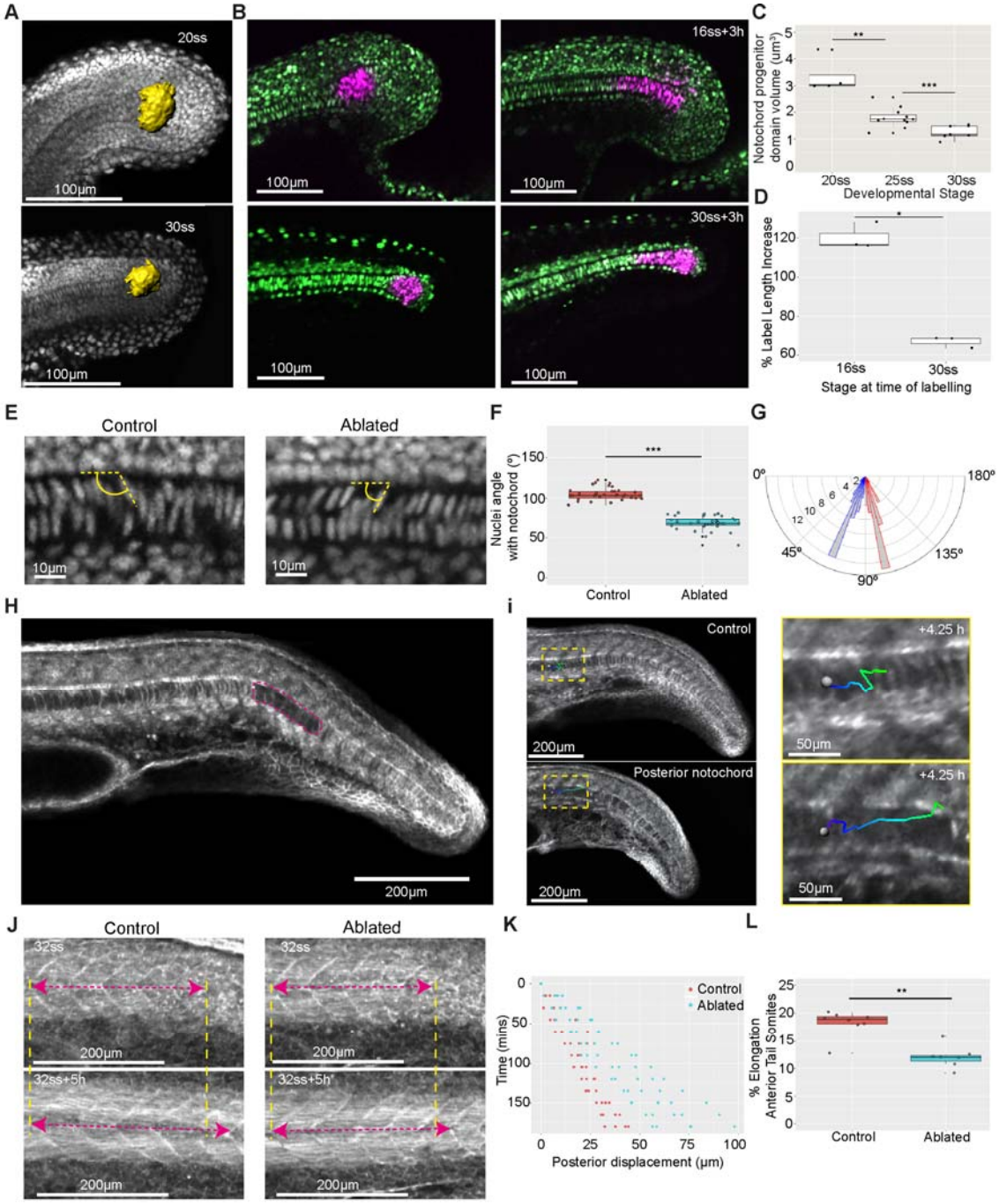

Fig. 4. Notochord progenitors provide a source of resistance to anterior notochord cell expansion that facilitates segmented tissue elongation in post-tailbud stage embryos.

(A) 3D surfaces of the notochord progenitor domain generated using *flh* gene expression in 20 and 30 somite stage embryos.
(B) Notochord progenitor photolabels in 16 and 30 somite stage embryos with corresponding images taken 3 hours after labelling.
(C) Notochord progenitor domain volume in μm^3 in 20, 25 and 30 somite stage embryos (n=5, n=13, n=7 embryos respectively, $p<0.01$, $p<0.001$ respectively).
(D) Photolabel AP length increase over 3 hours in 16 and 30 somite stage embryos (n=3 embryos per stage, $p<0.05$).
(E) Representative images of notochord nuclei located in the anterior tail region in control and ablated embryos.
(F) Boxplots showing angles between dorsally located nuclei and the notochord AP axis (º) in control and ablated embryos (n=7 embryos per condition, 5 angles measured per embryo, $p<0.001$).
(G) A histogram showing the distribution of angles between dorsally located nuclei and the notochord AP axis (º) in control and ablated embryos (n=7 embryos per condition, 5 angles measured per embryo, $p<0.001$).
(H) An embryo with a posterior notochord ablation.
(I) Manual tracking of expanding notochord cells in control embryos and embryos with a posterior notochord ablation.

(J) Elongation of a region of 5 anterior tail somites in control and posterior notochord ablated post-tailbud stage embryos.
(K) Notochord cell displacement over time in control and posterior notochord ablated embryos (n=4 and n=5 embryos respectively).
(L) Percentage elongation of a region of 5 anterior tail somites in control and posterior notochord ablated embryos (n=8 and n=7 embryos respectively, $p<0.01$)
Anterior is to the left and posterior to the right in all images.

Taken together, our findings show that notochord cell expansion generates a force, displacing neighbouring notochord cells relative to adjacent segmented tissue. In addition, unexpanded notochord cells in the posterior of the embryo provide resistance to notochord cell expansion, with removal of this posterior region increasing the posterior displacement rate of expanding notochord cells. Progenitors in the posterior add unexpanded cells to the posterior end of the notochord, thereby providing a source of resistance to notochord cell expansion as it progresses posteriorly along the axis (Fig. 5A). Given the progression of notochord cell expansion posteriorly along the axis, and the depletion of progenitors contributing cells to the posterior notochord over time, it is likely that the region providing resistance to notochord cell expansion will shrink as development progresses, and that the proportion of expanded cells in the notochord will increase relative to the proportion of unexpanded cells, until the entirety of the notochord is in an expanded state. Indeed, experiments in which the tail tip of larval stage embryos has been cut away reveal a rapid extrusion of notochordal tissue, suggesting that the posterior notochord no longer provides resistance at these stages (Romero et al., 2018).
We observe that somite elongation is decreased in embryos in which notochord cell expansion and the propagation of force along the notochord have been disrupted, leading us to propose that this force is translated into an AP directed stretch acting to elongate segmented tissue in post-tailbud stage embryos. This stretch may arise from the displacement of anterior and posterior regions of the notochord and somitic compartment away from one another as notochord cells expand (Fig. 5B).

Investigation into multi-tissue mechanical interactions in avian embryos has shown that, in contrast to the zebrafish, the presomitic mesoderm expands in volume leading to the lateral-to-medial compression and subsequent AP elongation of the notochord, displacing the tip of the notochord posteriorly into the tailbud and facilitating progenitor contribution to the axis (Bénazéraf et al., 2017; Steventon et al., 2016; Xiong et al., 2020). Our findings suggest that the notochord in zebrafish embryos contributes to axis elongation via a different mechanism that depends on the progressive expansion of notochord cells. In a similar case to that observed in amphibian embryos, cells in the zebrafish embryo notochord expand as they take in fluid (Adams et al., 1990). Studies approximating the notochord as a hydraulic skeleton have shown that such a system is capable of exerting force on its surroundings, but how such a force contributes to the tissue deformation required for axis elongation required further investigation (Koehl et al., 2000). In this study we

find that notochord cell expansion generates a force that deforms segmented tissue during post-tailbud stages of development, contributing to AP axis elongation. Whether this mechanism of axis elongation is utilised in the development of the chick embryo and other embryo species during later stages of development is an area for future investigation.

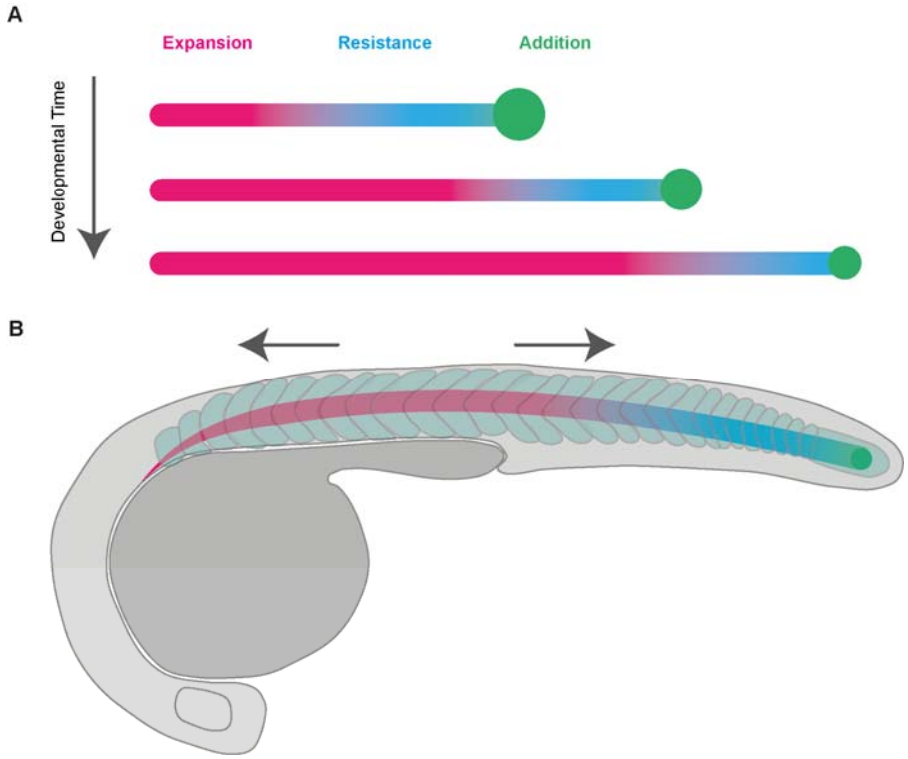

Fig. 5 Notochord cell expansion and addition of notochord cells from progenitors co-ordinates elongation of the AP axis.

(A) Notochord cell expansion progresses posteriorly along the axis and is resisted by a region of unexpanded notochord cells contributed by a pool of notochord progenitors. The notochord progenitor pool is depleted over time leading to a shift in the ratio of expanded to unexpanded cells in the notochord.
(B) Notochord cell expansion may be resisted in the anterior and posterior of the embryo, leading to an AP stretch along the somitic compartment.

Acknowledgements
We thank Andrea Dimitracopoulos, Fengzhu Xiong and Bertrand Benazeraf for critical reading of the manuscript, and members of the Steventon, Martinez-Arias and Franze group meetings for their support and feedback on the project. We also thank the PDN fish facility for their unwavering help and support with animal care and maintenance, and the CAIC imaging facility for their support with laser ablation experiments. B.S. was supported by a Henry Dale Fellowship jointly funded by the

Wellcome Trust and the Royal Society (109408/Z/15/Z) and S.M. was supported by the Wellcome Trust funded Developmental Mechanisms PhD programme.

Author Contributions

S.B.P.M. and B.S. conceived the project. S.B.P.M. carried out experiments and analysed the data. S.B.P.M. and B.S. wrote the manuscript.

Competing Interests

The authors declare no competing interests.

References

Adams, D. S., Keller, R. and Koehl, M. A. (1990). The mechanics of notochord elongation, straightening and stiffening in the embryo of Xenopus laevis. *Development* **110**, 115–130.

Attardi, A., Fulton, T., Florescu, M., Shah, G., Muresan, L., Lenz, M. O., Lancaster, C., Huisken, J., van Oudenaarden, A. and Steventon, B. (2018). Neuromesodermal progenitors are a conserved source of spinal cord with divergent growth dynamics. *Development* **145**, dev166728.

Bagwell, J., Norman, J., Ellis, K., Peskin, B., Hwang, J., Ge, X., Nguyen, S. V., McMenamin, S. K., Stainier, D. Y. and Bagnat, M. (2020). Notochord vacuoles absorb compressive bone growth during zebrafish spine formation. *Elife* **9**, 1840.

Bénazéraf, B., Beaupeux, M., Tchernookov, M., Wallingford, A., Salisbury, T., Shirtz, A., Shirtz, A., Huss, D., Pourquié, O., Francois, P., et al. (2017). Multi-scale quantification of tissue behavior during amniote embryo axis elongation. *Development* **144**, 4462–4472.

Choi, H. M. T., Beck, V. A. and Pierce, N. A. (2014). Next-generation in situ hybridization chain reaction: higher gain, lower cost, greater durability. *ACS Nano* **8**, 4284–4294.

Das, D., Jülich, D., Schwendinger-Schreck, J., Guillon, E., Lawton, A. K., Dray, N., Emonet, T., O'Hern, C. S., Shattuck, M. D. and Holley, S. A. (2019). Organization of Embryonic Morphogenesis via Mechanical Information. *Developmental Cell*.

Dray, N., Lawton, A., Nandi, A., Jülich, D., Emonet, T. and Holley, S. A. (2013). Cell-fibronectin interactions propel vertebrate trunk elongation via tissue mechanics. *Curr. Biol.* **23**, 1335–1341.

Ellis, K., Bagwell, J. and Bagnat, M. (2013). Notochord vacuoles are lysosome-related organelles that function in axis and spine morphogenesis. *The Journal of Cell Biology* **200**, 667–679.

Gomez, C., Özbudak, E. M., Wunderlich, J., Baumann, D., Lewis, J. and Pourquié, O. (2008). Control of segment number in vertebrate embryos. *Nature* **454**, 335–339.

Goto, H., Kimmey, S. C., Row, R. H., Matus, D. Q. and Martin, B. L. (2017). FGF and canonical Wnt signaling cooperate to induce paraxial mesoderm from tailbud neuromesodermal progenitors through regulation of a two-step epithelial to mesenchymal transition. *Development* **144**, 1412–1424.

Kanki, J. P. and Ho, R. K. (1997). The development of the posterior body in zebrafish. *Development* **124**, 881–893.

Kimmel, C. B., Ballard, W. W., Kimmel, S. R., Ullmann, B. and Schilling, T. F. (1995). Stages of embryonic development of the zebrafish. *Dev. Dyn.* **203**, 253–310.

Koehl, M., Quillin, K. J., Pell, C. A. (2000) Mechanical Design of Fiber-Wound Hydraulic Skeletons: The Stiffening and Straightening of Embryonic Notochords. *Amer. Zool.* **40,** 28-41

Lawton, A. K., Nandi, A., Stulberg, M. J., Dray, N., Sneddon, M. W., Pontius, W., Emonet, T. and Holley, S. A. (2013). Regulated tissue fluidity steers zebrafish body elongation. *Development* **140**, 573–582.

Mongera, A., Rowghanian, P., Gustafson, H. J., Shelton, E., Kealhofer, D. A., Carn, E. K., Serwane, F., Lucio, A. A., Giammona, J. and Campàs, O. (2018). A fluid-to-solid jamming transition underlies vertebrate body axis elongation. *Nature* **561**, 401–405.

Oates, A. C., Morelli, L. G. and Ares, S. (2012). Patterning embryos with oscillations: structure, function and dynamics of the vertebrate segmentation clock. *Development* **139**, 625–639.

Romero, M. M. G., McCathie, G., Jankun, P. and Roehl, H. H. (2018). Damage-induced reactive oxygen species enable zebrafish tail regeneration by repositioning of Hedgehog expressing cells. *Nat Commun* **9**, 1–11.

Rost, F., Eugster, C., Schröter, C., Oates, A. C. and Brusch, L. (2014). Chevron formation of the zebrafish muscle segments. *Journal of Experimental Biology* **217**, 3870–3882.

Row, R. H., Tsotras, S. R., Goto, H. and Martin, B. L. (2016). The zebrafish tailbud contains two independent populations of midline progenitor cells that maintain long-term germ layer plasticity and differentiate in response to local signalling cues. *Development* **143**, 244–254.

Seleit, A., Gross, K., Onistschenko, J., Woelk, M., Autorino, C. and Centanin, L. (2020). Development and regeneration dynamics of the Medaka notochord. *Developmental Biology* **463**, 11–25.

Stemple, D. L. (2005). Structure and function of the notochord: an essential organ for chordate development. *Development* **132**, 2503–2512.

Steventon, B., Duarte, F., Lagadec, R., Mazan, S., Nicolas, J.-F. and Hirsinger, E. (2016). Species-specific contribution of volumetric growth and tissue convergence to posterior body elongation in vertebrates. *Development* **143**, 1732–1741.

Tlili, S., Yin, J., Rupprecht, J. F., Mendieta-Serrano, M. A., Weissbart, G., Verma, N., Teng, X., Toyama, Y., Prost, J. and Saunders, T. E. (2019). Shaping the zebrafish myotome by intertissue friction and active stress. *Proc Natl Acad Sci USA* **116**, 25430–25439.

Xiong, F., Ma, W., Bénazéraf, B., Mahadevan, L. and Pourquié, O. (2020). Mechanical Coupling Coordinates the Co-elongation of Axial and Paraxial Tissues in Avian Embryos. *Developmental Cell* **55**, 1-13.

Materials and Methods

Zebrafish strains and maintenance

This research was regulated under the Animals (Scientific Procedures) Act 1986 Amendment Regulations 2012 following ethical review by the University of Cambridge Animal Welfare and Ethical Review Body (AWERB).
Adult Zebrafish (Danio rerio) and embryos were reared at 28°C and staged using the number of somites. Wildtype embryos used in this study were of the TL strain. Prior to live imaging embryos were anaesthetised with tricaine (MS-222).
The following zebrafish lines were used in this study; H2B-GFP, Tg(actb2:Lifeact-EGFP), and pNtl:Kaede[16].

Timelapse Live Imaging

Embryos were mounted in 3% Methylcellulose to hold embryos still whilst allowing movement of the tail and ensuring embryos could continue to develop normally. Embryos were mounted in glass bottom dishes (MatTek), with the head and yolk submerged in methylcellulose but with the tail freed of methylcellulose. Embryos were submerged in E3 media. An eyelash tool was used to reposition embryos in the methylcellulose so that they were lying flat on the bottom of the dish. Dishes with mounted embryos were transferred to a Zeiss LSM 700 confocal microscope equipped with a heated chamber set to 28°C. A 10x air objective (NA=0.45) was used to capture the whole body of developing embryos for timelapse movies spanning 5 or more hours.

Drug treatments

Bafilomycin A1 (Sigma Aldrich) was used to inhibit vacuolation in the notochord of developing zebrafish embryos. 16ss embryos were submerged in E3 media with Bafilomycin at a final concentration of 0.5uM. Embryos were then incubated for 6 hours at 28°C. For visualisation of vacuolation in the notochord Lifeact-GFP embryos were imaged live using a 10x air objective after 6 hours of incubation. Live imaging of somite elongation in DMSO and Bafilomycin treated embryos was performed using the pNtl:kaede line using a multi-well chamber.

Photolabelling

Wild-type Zebrafish embryos were injected with approximately 200 pg of nuclear-targeted Kikume at the one-cell stage and incubated in the dark until the required developmental stage was reached. Embryos were mounted and transferred to the microscope as described above for live imaging. For notochord cell movement analysis, rectangular stripes were defined along the embryo. Photoconversion of NLS-KikGR was performed whilst using a 20x air objective and scanning the 405 nm laser at 11% power within defined regions. Photolabelling was confirmed by simultaneously visualing both NLS-KikGR emissions using the 488 nm and 561nm lasers.

Hybridisation Chain Reaction (HCR)

HCR was used to visualise gene expression in fixed embryos. HCR has been described here (Choi et al., 2014). Briefly, Embryos where fixed in 4% PFA overnight at 4°C at the required developmental stage. Embryos where then dehydrated into 100% methanol, stored overnight at -20°C, and then rehydrated into PBST when the HCR was to be carried out. Once rehydrated, embryos where prehybridized in 30% probe hybridisation buffer at 37°C and then incubated overnight at 37°C with probes for the desired mRNA transcript detection. Embryos where then washed with SSCT at room temperature and pre-amplified in amplification buffer. Embryos where then incubated overnight (in the dark) at room temperature with hairpins specific to the probes to fluorescently label the mRNA transcripts. After this the embryos were washed with SSCT and incubated with DAPI overnight at 4°C and then washed with SSCT before imaging the next day.

The notochord progenitor domain was visualised using probes targeted to the gene noto (also known as flh).

Photoablation

Laser ablation was performed using a TriM Scope II Upright 2-photon scanning fluorescence microscope equipped with a tunable near-infrared laser. Inspector Pro software was used to control the microscope and a laser power of approximately 1.3W was used for ablation.

Notochord ablations were carried out using a lifeact-GFP reporter line to visualise notochord cells and ablations were performed in the plane of the notochord.

For notochord progenitor ablations the morphology of the notochord progenitor cell population was used to determine the location of the notochord progenitors. Ablations were carried out to ensure as many of the notochord progenitors as possible were ablated, without ablating any other progenitor types.

Image processing and analysis

Images were processed either in ImageJ/Fiji or Imaris.

Length and curvature measurements

For length and curvature measurements the ImageJ plug-in ‘Kappa’ was used. A maximum projection of the nuclear-GFP of Lifeact-GFP channel was used so that somites could be visualised and used as landmarks to define the segmented and unsegmented regions. The segmented region in tailbud and post-tailbud stage embryos was defined as the 5 somites located in the anterior tail region (approximately at the end of the yolk extension). The unsegmented region in both tailbud and post-tailbud stage embryos was defined as the region spanning from the most posterior clearly segmented somite boundary to the end of the tail. Embryo side views were used to measure the curvature and length of regions of the axis. Trunk curvature was measured by drawing a line with 6 points through the middle of the trunk as viewed from the side. This was then converted into a spline, and the points were adjusted so that a smooth curve fitting the curvature of the embryo region

passed through the midpoint of that region. Tail curvature was measured in a similar fashion, however in this case 4 points were used to create a curve passing through the midpoint of the tail. The average curvature was used for comparing the curvature of these regions in multiple embryos of different stages. To visualise the curvature profile along the whole somitic compartment in embryos of different stages, a spline passing from the anterior tip to the posterior tip of the somitic compartment was generated, and point curvature was used to generate a heatmap in order to visualise the curvature profile along the axis.

Notochord progenitor domain volume

To measure the volume of the notochord progenitor domain at different developmental stages noto gene expression was visualised using HCR and acquisition of confocal z-stacks of fixed 20ss, 25ss, and 30ss embryo tails. These images were imported into imaris, allowing easy visualisation in 3D. The 'surfaces' function in imaris was then used to generate a surface around the noto gene expression signal, with surface volume given as an output.

Vacuole AP length measurements

The 'oblique slicer' tool in imaris was used to find a plane that passed through the middle of the notochord where the total length and height of vacuoles could be properly visualised. The 'measurements' tool was used to make two point per vacuole defining a line passing through the greatest AP length of the vacuole. Line lengths were calculated using an inbuilt function in imaris.

Data analysis

Data was stored in excel spreadsheets and analysis was performed using the programming language 'Python'. All data plots were generated in Python using the ggplot library. Box plots show the median, upper and lower quartiles, and whiskers represent 1.5 times the interquartile distance. All data points were shown and included in statistical analyses.

Statistical Analysis

The Mann-Whitney U nonparametric statistical test was used to test whether two independent samples came from populations with the same distribution. This test was implemented in python using the scipy.stats.mannwhitneyu() function.
The Kruskal-Wallis nonparametric statistical test was used to test whether more than two independent samples came from populations with the same distribution. Pairwise comparisons between samples were performed in a post-hoc fashion to identify whether compared samples came from populations with the same distribution. The Kruskal-Wallis test was implemented using the stats.kruskal() function, and the post hoc test was implemented with the sp.posthoc_conover() function.
In all cases a p-value of <0.05 was taken as a threshold for significance.

Supplementary information

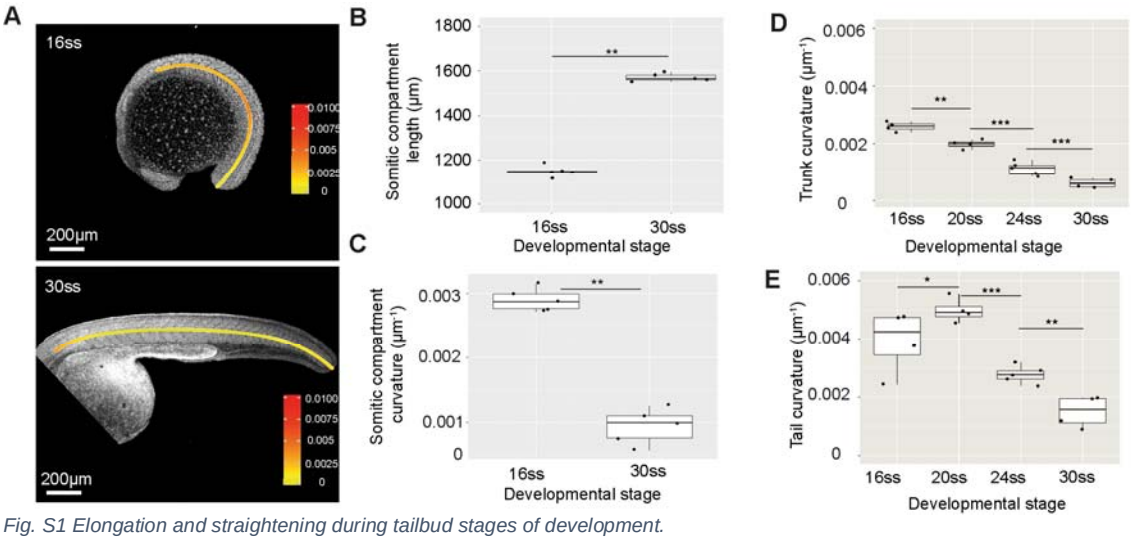

Fig. S1 Elongation and straightening during tailbud stages of development.

(A) Representative images of live 16 and 30 somite stage embryos. Overlaid curves indicate region used for somitic compartment length and curvature measurements. Heatmap shows point curvature.
(B) Somitic compartment length in 16 and 30 somite stage embryos (n=5 per stage, $p<0.01$).
(C) Somitic compartment length in 16 and 30 somite stage embryos (n=5 per stage, $p<0.01$).
(D) Trunk curvature in 16, 20, 24 and 30 somite stage embryos (n=4,4,5,4 embryos respectively per stage, $p<0.01$, $p<0.001$, $p<0.001$ respectively).
(E) Tail curvature in 16, 20, 24 and 30 somite stage embryos (n=4,4,5,4 embryos respectively per stage, $p<0.05$, $p<0.001$, $p<0.01$ respectively).

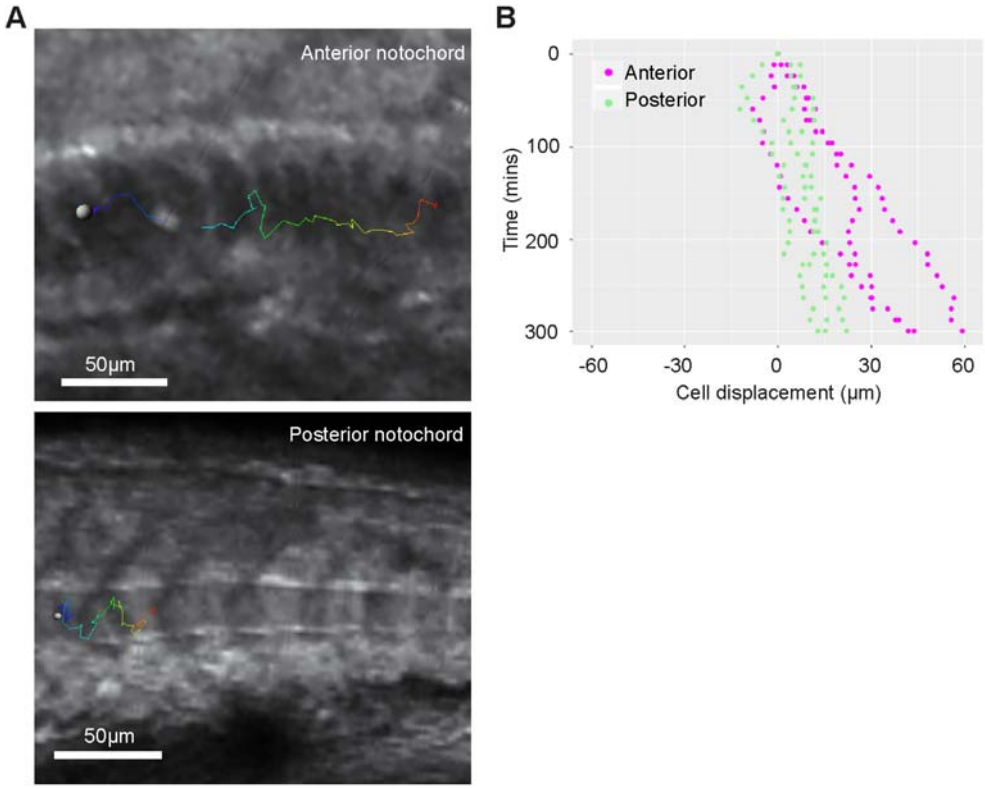

Fig. S2 Notochord cell displacement relative to adjacent somites in expanded and unexpanded notochord regions.

(A) Notochord cell tracks in an anterior expanded region and a posterior unexpanded region.
(B) Notochord cell displacement over time in expanded trunk regions and unexpanded tail regions (n= 3 embryos).

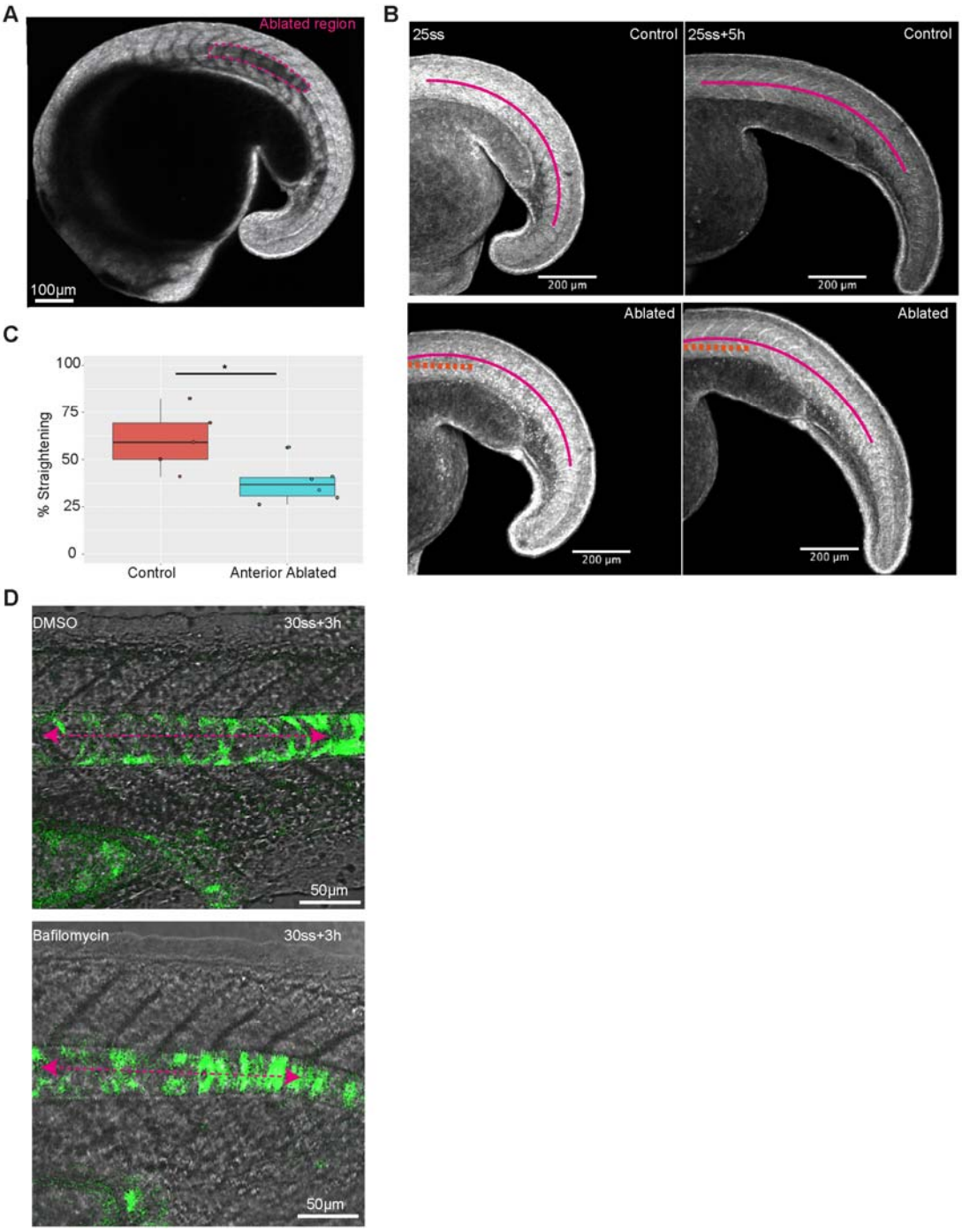

Fig. S3 Notochord cell expansion impacts embryo straightening and elongation.

(A) Representative image of an embryo with a region of anterior notochord ablated just as vacuoles are beginning to expand.
(B) Images of control and anterior notochord ablated embryos at the 25 somite stage and 5 hours later. Overlaid curves show the region tracked over time for curvature measurements.
(C) Percentage straightening (decrease in curvature) over 5 hours in control and ablated tailbud stage embryos (n=5 control and 6 ablated embryos, $p<0.05$).
(D) A region of 5 anterior tail somites in control and bafilomycin treated embryos imaged 3 hours after the 30 somite stage.

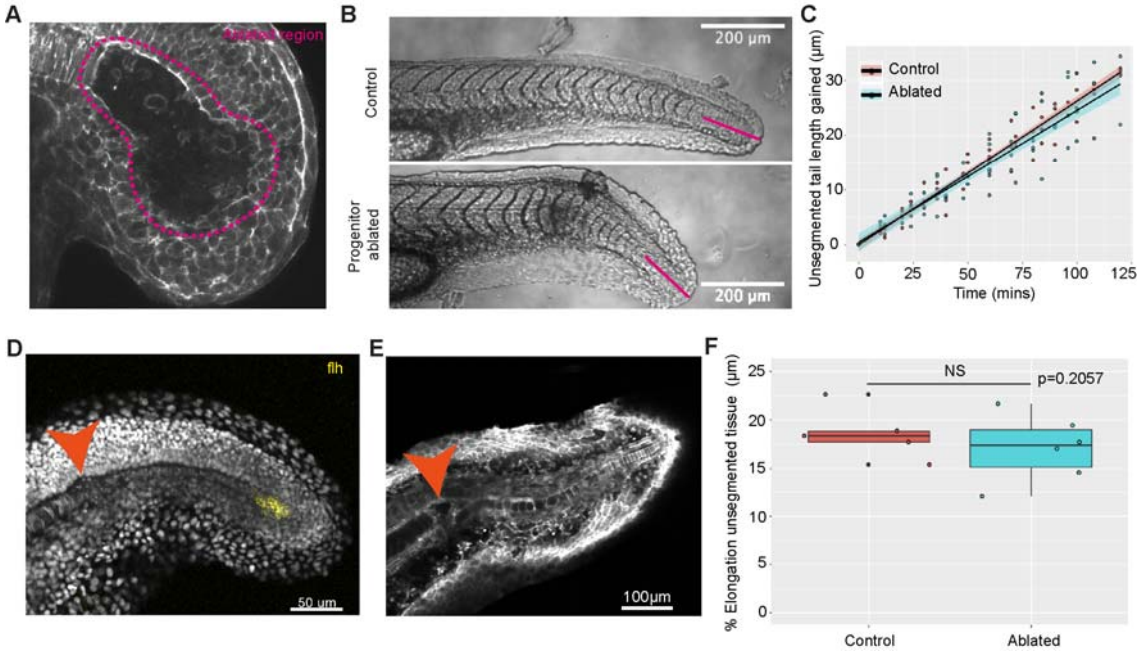

Fig. S4 Notochord progenitors regenerate after ablation and recover the posterior notochord.

(A) Representative image of a 16-somite stage embryo with notochord progenitors ablated.
(B) Representative images of control and progenitor ablated post-tailbud stage embryos. The magenta line indicates the length of a small region of residual unsegmented tissue tracked over time.
(C) Length gain in a small region of unsegmented tissue over time in control and progenitor ablated post-tailbud stage embryos (n=6 control and n=7 ablated embryos).
(D) Representative image of an embryo fixed approximately 5 hours after notochord progenitor ablation. The gene expression marker 'flh' marks the notochord progenitors.
(E) Representative image of an embryo imaged approximately 24 hours after notochord progenitor ablation. The recovered notochord is visualised using a lifeact-GFP reporter.
(F) Percentage elongation of unsegmented tissue in the tail region after recovery from notochord progenitor ablation over approximately 100 minutes (n=5 control and n=6 ablated embryos, p=0.2057).
Orange arrows indicate the internalised ablated tissue.